# Design and analysis of dual wound machine for electric ships

Boyuan Yin[1], Xiaoze Pei[1], Xianwu Zeng[2], Fred Eastham[1], Chris Hodge[3], Oliver Simmonds[3]

***Abstract*—Integrated full electric propulsion (IFEP) systems eliminate the direct mechanical coupling between the prime mover and the propeller, enabling easier connection of multiple prime movers and allowing more equitable and fuel-efficient engine loading. These features are important in both cruise ship and naval warship design. Propulsion and ship service systems require different electrical ratings. The general solution is to use multiple electrical machine sets. To approach the most compact design and maximise the weight reduction, a dual wound machine is considered in this paper. It has dual two-layer windings which share the same slots and uses one prime mover, to produce two independent power supplies. This paper designs a dual wound machine with no electromagnetic coupling due to the airgap fields, by algebraically analyzing the harmonic distribution. Further verification of the nil electro-magnetic coupling due to both the airgap and slot leakage fluxes is provided by 2D finite element modeling. Both loaded and unloaded conditions are considered.**

***Keywords*—Dual wound machine, Electric ship, Harmonic decoupling, Independent power supplies.**

## I. INTRODUCTION

Traditional large cruise ships and naval warships contain a set of diesel generators for ship service systems, and separate prime overs for propulsion [1], [2]. Electric propulsion has emerged as the most efficient arrangement for several vessel types [3], [4], and the number of electrically propelled ships has grown rapidly over the last ten years [5]. Compared with direct-drive diesel systems, electric propulsion has great potential to reduce fuel consumption, enhance dynamic performance and increase the system reliability [6]-[8]. Integrated full electric propulsion (IFEP) systems remove the direct mechanical coupling between the prime mover and propeller, and build all-electric networks, which can support both the ship services and propulsion segments [9]. IFEP benefits the ship structure by:

1. The arrangement of engines on the ship becomes more flexible because the connection between the diesel machines and the propulsion is eliminated.
2. All engines providing electrical power helps to decrease the total number of engines, which contributes to the reduction of the weight and volume for the ship, as well as the noise and vibration.
3. Independent engine groups and propulsion machines can use more commercial solutions for maintenance and to decrease capital costs.

Based on the IFEP system, this paper proposes the design of a dual wound machine providing the power for both ship services and the propulsion segment simultaneously. Some studies of dual wound machine generators have been performed in [10]-[12]. Compared with the general IFEP system, a dual wound machine only requires one prime mover (diesel engine) with less volume and mass than two separate diesel engines to the same total power rating, saving space on the ship [13]. With only one electric machine, there is no integration problem between generators. The two outputs of the dual wound machine are from two windings on the stator, which share the same slots but can be windings of different forms. However the stator winding arrangements must eliminate the electromagnetic coupling between them to avoid cross-coupling between the supplies. In addition, each of the two rotor windings needed should couple with only the stator winding for which it is intended. There are different winding strategies applied to dual wound machines [14], [15]. In addition, the harmonic analysis of the windings has been studied in [16]-[18]. Dual wound machines are shown to have great potential to provide better power quality [15], better torque quality [19] and reduce the losses [20].

This paper designs a model 2 and 6-pole dual wound machine with 5 kW output using an existing machine frame. An analytical harmonic calculation is presented which shows that there is no electromagnetic coupling due to the airgap fields. The magnetic flux density distribution and operational performance are also analyzed by 2D finite element modelling in COMSOL. This further verifies that there is no electro-magnetic coupling between the two sets of stator windings due to both air gap and slot leakage fluxes. This paper is structured as follows: Section II introduces the dual wound machine topology and dimension using an existing machine frame; Section III shows the rotor winding distributions and the magnetic flux density in the air gap; Section IV presents the stator electro-magnetic decoupling and winding harmonic analysis; Section V demonstrates the load operation and further demonstrates the independence of the two power supplies.

## II. DUAL WOUND MACHINE TOPOLOGY

The model dual wound machine designed in this paper is based on an existing machine frame at the University of Bath. Table I presents its dimension.

TABLE I MACHINE DIMENSION

| Item | Stator | Rotor |
|---|---|---|
| Number of slots | 36 | 24 |
| Diameter | 190.5 mm | 186.5 mm |
| Axial length | 123.6 mm | 139.5 mm |
| Slot opening | 2.7 mm | 3.5 mm |
| Airgap | 2 mm | |
| Stator outer diameter | 295 mm | |

[1]Dept. of Electronics & Electrical Engineering, University of Bath.
[2]Dept. of Mechanical Engineering, University of Bath.
[3]BMT Defence & Security UK Ltd.

## III. AIR GAP FLUX DENSITY PRODUCED BY THE ROTOR WINDINGS

The excitation magnetic flux density in the air gap is produced by the windings in the rotor slots. In order to generate a good approximation to a sinusoidal magnetic field, concentric windings are used. The coils are series connected and due to the different number of conductors in each slot, the winding produces the required reasonable approximation to a sinusoidal air gap flux distribution. Since the rotor has 24 slots, the 2-pole winding needs a pole pitch of 12 slots and the 6-pole 4 slots. The coil distributions are shown in Fig. 1, which shows the 2-pole distribution (one coil set out of two) at Fig. 1(a) and the six-pole distribution (two coil sets out of six) at Fig. 1(b). Each of these coil sequences are repeated.

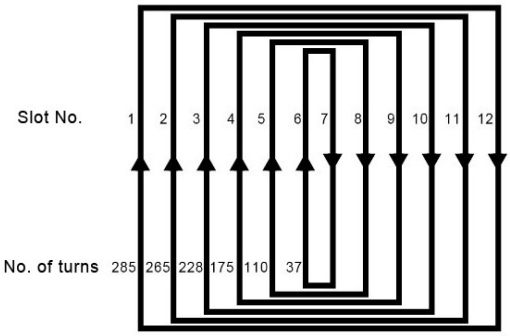


(a) 2-pole rotor winding diagram (one coil set of two)

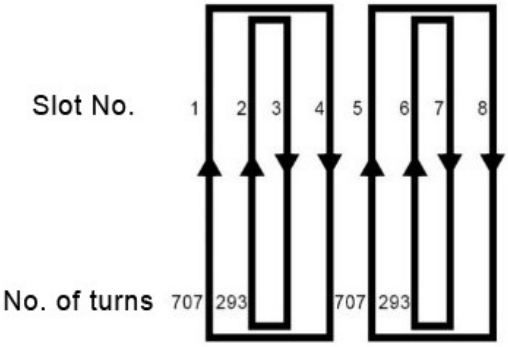


(b) 6-pole rotor winding diagram (two coil sets of six)

Fig. 1. Rotor winding diagram

Table II and Table III show the magnetic field harmonic distribution of the 2-pole and 6-pole rotor windings. They show that there are no common harmonics between the two windings, which means they have no mutual coupling. This is important since it implies that when changing the dc current level in one winding transient emfs will not be induced in the other. The calculations are performed using the method given in [16]. It should be noted that the calculated range was up to the 35th harmonic.

TABLE II 2-POLE ROTOR MAGNETIC FIELD HARMONICS DISTRIBUTION

| Harmonics | Magnetic field (T) |
|---|---|
| 1 | 0.603 |
| 23 | 0.026 |
| 25 | 0.024 |

TABLE III 6-POLE ROTOR MAGNETIC FIELD HARMONICS DISTRIBUTION

| Harmonics | Magnetic field (T) |
|---|---|
| 3 | 0.536 |
| 21 | 0.077 |
| 27 | 0.060 |

Each rotor coil produces a square wave of flux density, so that when all the coil contributions are added together the approximate sinusoidal magnetic flux density distribution is as shown in Fig. 2. Given that the number of slots per pole is larger the 2-pole rotor magnetic field in the air gap (Fig.2(a)) is smoother than 6-pole winding (Fig. 2(b)). The ripples appearing in the waves are caused by the slotting.

The rotor winding distributions could start at any phase position with respect to each other. The best position can be taken as that which produces the smallest total field. A study was performed to minimize the total field produced when both windings are excited. This involved changing the relative position of the windings by one slot at a time Fig. 3 shows the total field at the best position when the 2-pole and 6-pole windings are aligned. The he finite element modelling in this paper is based on this aligned position.

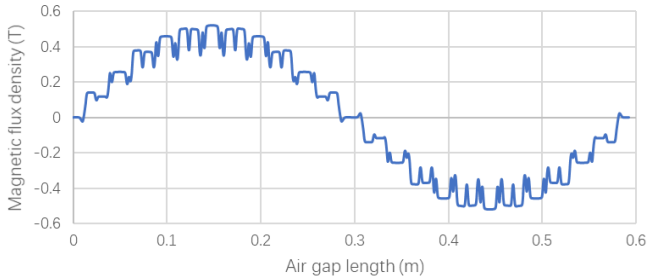


(a) 2-pole rotor magnetic flux density

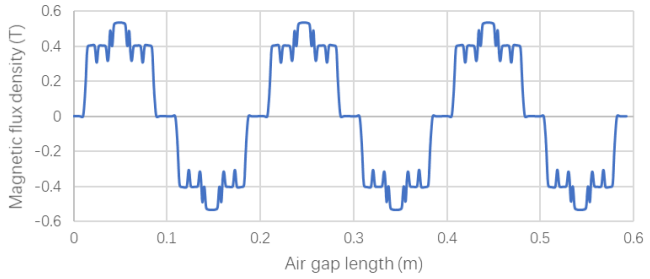


(b) 6-pole rotor magnetic flux density

Fig. 2. Rotor magnetic flux density distribution in the air gap

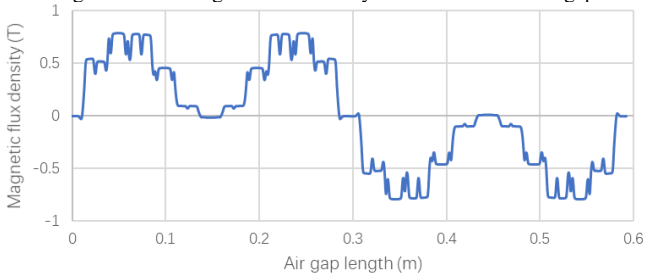


Fig. 3. 2-pole and 6-pole magnetic flux density when it is aligned

## IV. WINDING HARMONICS & ELECTRO-MAGNETIC COUPLING

The stator windings produce induced emf from the magnetic flux density provided by the rotor windings. The frequency of the output voltage is proportional to pole number so the 6-pole winding produces 3 times the frequency of the 2-pole. The 2-pole and 6-pole windings share the same 36 slots on the stator frame as shown in Fig. 4, each pole winding occupies two layers, one above the other, so there are four layers in total. The arrangement aims to maximise the induced voltage and minimise the space harmonic from the windings whilst ensuring that there is no electromagnetic coupling between them.

Fig.4. shows the chosen solution. The 2-pole and 6-pole

windings are both short-pitched the 2-pole has pitch angle of 120° and the 6-pole 150°.

It is worth noting that since the 2 and 6-pole fields rotate at the same speed as the rotor, the relative position between the air gap fluxes of the 2-pole and 6-pole windings, which depends on the power factor of the loads, is therefore constant. The stator windings used the same aligned position as the rotor windings assuming that the load power factor is the same. Further study could be done if the two load power factors are known.

| Slot | 1 | 2 | 3 | 4 | 5 | 6 | 7 | 8 | 9 | 10 | 11 | 12 | 13 | 14 | 15 | 16 | 17 | 18 | 19 | 20 | 21 | 22 | 23 | 24 | 25 | 26 | 27 | 28 | 29 | 30 | 31 | 32 | 33 | 34 | 35 | 36 |
|---|---|---|---|---|---|---|---|---|---|---|---|---|---|---|---|---|---|---|---|---|---|---|---|---|---|---|---|---|---|---|---|---|---|---|---|---|
| 2 Pole | R | R | R | R | R | R | -B | -B | -B | -B | -B | -B | Y | Y | Y | Y | Y | Y | -R | -R | -R | -R | -R | -R | B | B | B | B | B | B | -Y | -Y | -Y | -Y | -Y | -Y |
| | -B | -B | -B | -B | -B | -B | Y | Y | Y | Y | Y | Y | -R | -R | -R | -R | -R | -R | B | B | B | B | B | B | -Y | -Y | -Y | -Y | -Y | -Y | R | R | R | R | R | R |
| 6 Pole | R | R | -B | -B | Y | Y | -R | -R | B | B | -Y | -Y | R | R | -B | -B | Y | Y | -R | -R | B | B | -Y | -Y | R | R | -B | -B | Y | Y | -R | -R | B | B | -Y | -Y |
| | R | -B | -B | Y | Y | -R | -R | B | B | -Y | -Y | R | R | -B | -B | Y | Y | -R | -R | B | B | -Y | -Y | R | R | -B | -B | Y | Y | -R | -R | B | B | -Y | -Y | R |

Fig. 4. Stator winding distribution

The dual wound machine is expected to generate independent supplies. The flux density can only couple with the windings that have the same pole number. At the same time, the current in a winding can only produce fluxes corresponding to its winding harmonics. It therefore follows that to avoid electromagnetic coupling between the windings there should be no common winding harmonics

Table IV and Table V show the winding harmonics of 2-pole stator winding and 6-pole stator winding. It can be seen that there are no common harmonics between the two windings, fulfilling the condition for no mutual coupling, and ensuring that the two outputs are independent. The calculations are performed using the method given in [16]. Using this technique, the windings are represented by harmonic, equivalent, positive negative and zero winding sequence sets which when supplied from 3 phase currents produce forward backward and stationary fields. It is also important that a rotor winding couples only with its corresponding stator winding. And it can be seen from Table II and Table V, Table III and Table IV, there are no rotor harmonics that couple with the inappropriate stator winding.

TABLE IV 2-POLE STATOR WINDING HARMONICS DISTRIBUTION

| Harmonics | PPS | NPS | ZPS |
|---|---|---|---|
| 1 | 0.83 | 0.00 | 0.00 |
| 5 | 0.00 | 0.17 | 0.00 |
| 7 | 0.13 | 0.00 | 0.00 |
| 11 | 0.00 | 0.09 | 0.00 |
| 13 | 0.08 | 0.00 | 0.00 |
| 17 | 0.00 | 0.07 | 0.00 |
| 19 | 0.07 | 0.00 | 0.00 |
| 23 | 0.00 | 0.08 | 0.00 |
| 25 | 0.09 | 0.00 | 0.00 |
| 29 | 0.00 | 0.13 | 0.00 |
| 31 | 0.17 | 0.00 | 0.00 |
| 35 | 0.00 | 0.83 | 0.00 |

*PPS – Positive phase sequence
NPS – Negative phase sequence
ZPS – Zero phase sequence

TABLE V 6-POLE STATOR WINDING HARMONICS DISTRIBUTION

| Harmonics | PPS | NPS | ZPS |
|---|---|---|---|
| 3 | 0.93 | 0.00 | 0.00 |
| 9 | 0.00 | 0.00 | 0.50 |
| 15 | 0.00 | 0.07 | 0.00 |
| 21 | 0.07 | 0.00 | 0.00 |
| 27 | 0.00 | 0.00 | 0.50 |
| 33 | 0.00 | 0.93 | 0.00 |

A 2D finite element simulation using COMSOL has been performed to verify the above results for both the airgap fluxes considered by the harmonic analysis and the slot leakage fluxes. Fig. 5 and Fig. 6 present the condition when only the 2-pole rotor winding is excited. Fig. 5 shows the magnetic flux density and magnetic vector potential distributions. Under this condition, the 2-pole stator winding generates induced voltage as shown in Fig. 6(a) while the 6-pole stator winding has zero voltage as presented in Fig. 6(b). It is worth mentioning that the end winding resistance and reactances are not considered in this paper (requiring a 3D model) but will be included in the future work.

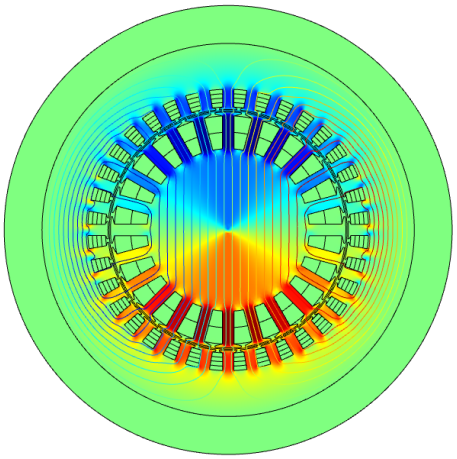

Fig. 5. 2-pole magnetic field distribution

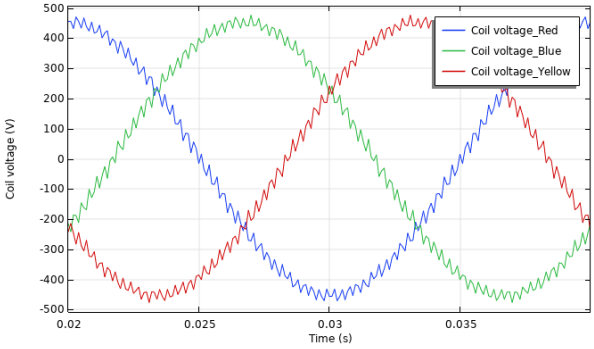


(a) 2-pole stator voltage with 2-pole excitation

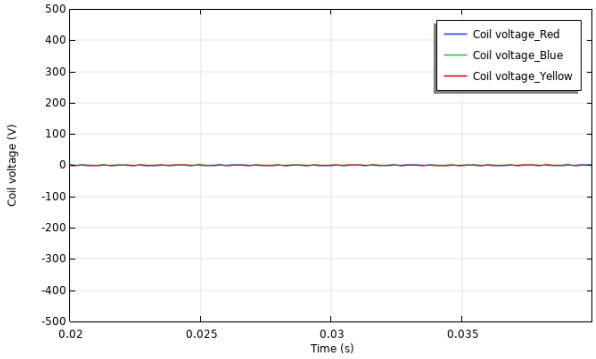


(b) 6-pole stator voltage with 2-pole excitation

Fig. 6. 2-pole and 6-pole stator voltage with 2-pole excitation

Fig. 7 and Fig. 8 present the simulation results when only the 6-pole rotor winding excited. Fig. 7 presents the 6-pole magnetic flux and magnetic vector potential distributions. It is clear that 2-pole winding has no induced emf, while the 6-pole winding produces sinusoidal induced emf only when 6-pole rotor winding is excited.

When both windings are excited, the combined magnetic flux density and magnetic vector potential distributions are shown in Fig. 9. Fig. 10 clearly indicates that the induced voltage is independently generated in the 2-pole and 6-pole

windings. It is to be concluded that the excitation of 6-pole rotor winding has a negligible impact on 2-pole stator winding, and vice versa.

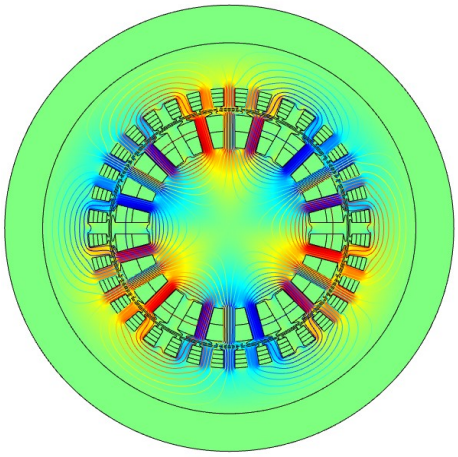

Fig. 7. 6-pole magnetic field distribution

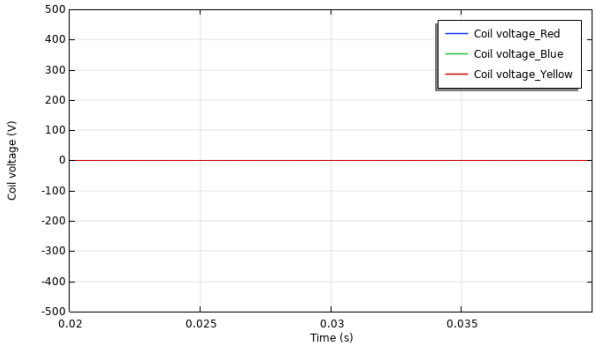


(a) 2-pole stator voltage with 6-pole excitation

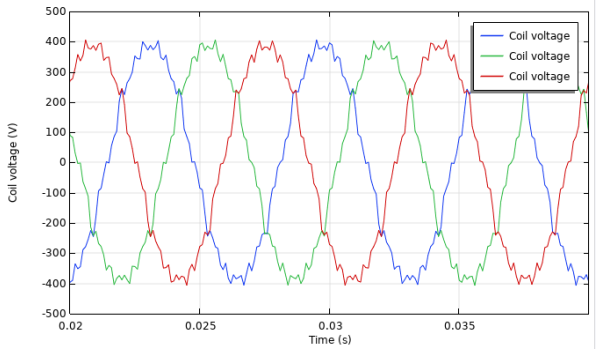


(b) 6-pole stator voltage with 6-pole excitation

Fig. 8. 2-pole and 6-pole stator voltage with 6-pole excitation

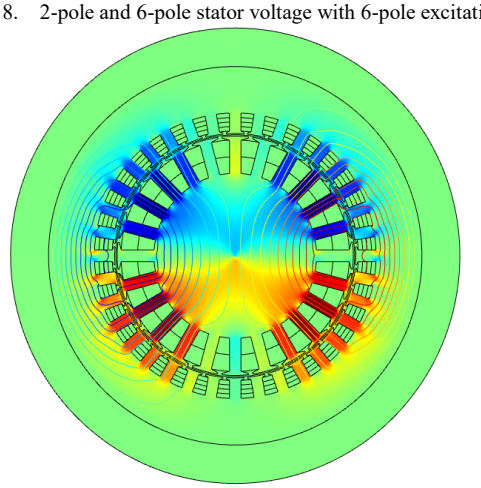

Fig. 9. 2-pole and 6-pole magnetic field distribution

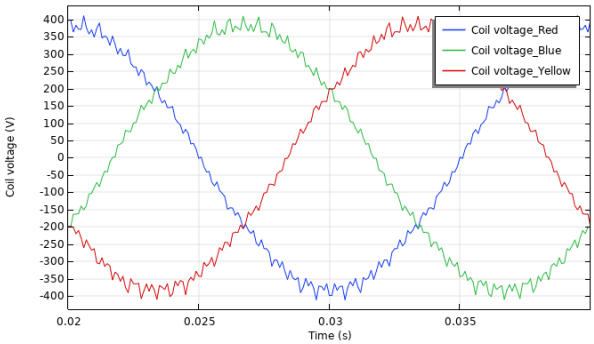


(a) 2-pole stator voltage with 2-pole and 6-pole excitation

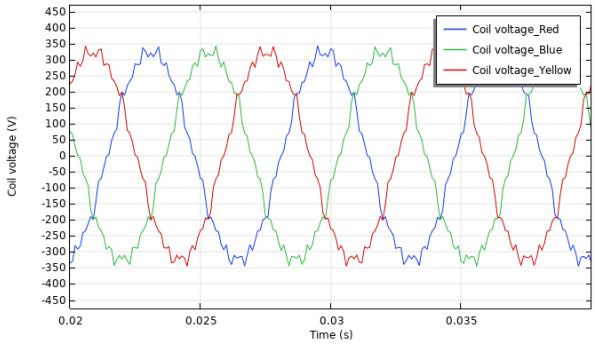


(b) 6-pole stator voltage with 2-pole and 6-pole excitation

Fig. 10. 2-pole and 6-pole stator voltage with 2-pole and 6-pole excitation

## V. MODELLING PERFORMANCE WITH RESISTIVE LOAD

To simulate the load operation performance and further demonstrate the fully decoupled winding properties, a resistive load study has been carried out. This simulation aims to verify that the 2-pole and 6-pole windings are able to operate independently regardless of the other winding, when both 2-pole and 6-pole rotor windings are energized. The power rating of the 2-pole machine is designed to be 3 kW. The phase voltage and current are assumed to be 240 $V_{rms}$ and 4 $A_{rms}$. The load resistance for the 2-pole machine is therefore 60 Ω. For the 6-pole machine, the power rating is designed to be 2 kW. The phase voltage and current are assumed to be 240 $V_{rms}$ and 3 $A_{rms}$ so that the load resistance for the 6-pole machine is 80Ω. Fig. 11 presents the terminal voltage and current for both windings when the 2-pole stator winding feeds a 60 Ω resistive load and 6-pole stator winding is on open circuit. It can be observed that the 2-pole winding works under rated condition while 6-pole winding produces induced voltage but has no current.

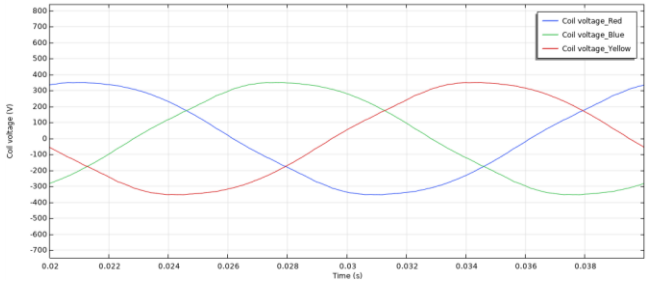


(a) 2-pole stator terminal voltage with 2-pole loaded

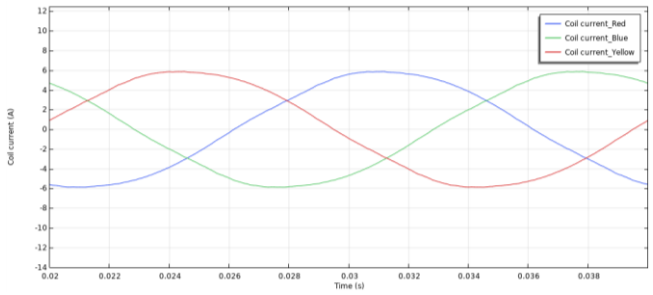


(b) 2-pole stator terminal current with 2-pole loaded

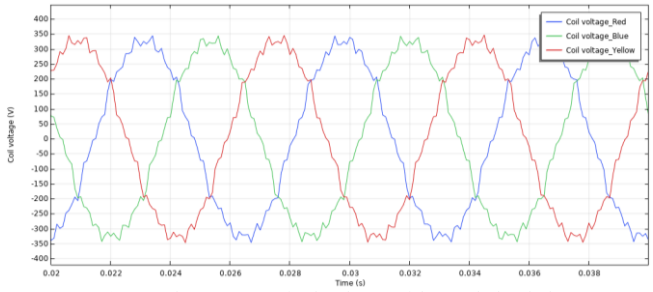


(c) 6-pole stator terminal voltage with 2-pole loaded

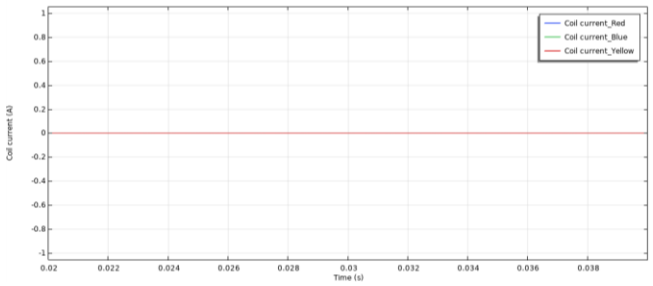


(d) 6-pole stator terminal current for 2-pole loaded

Fig. 11. Terminal voltage & current with 2-pole loaded

Fig. 12 shows the 2-pole winding on open circuit and 6-pole winding with a resistive load of 80 Ω. Combined with the 2-pole loaded result in Fig. 11, it is confirmed that the 2-pole and 6-pole windings will work separately under their respective rated conditions.

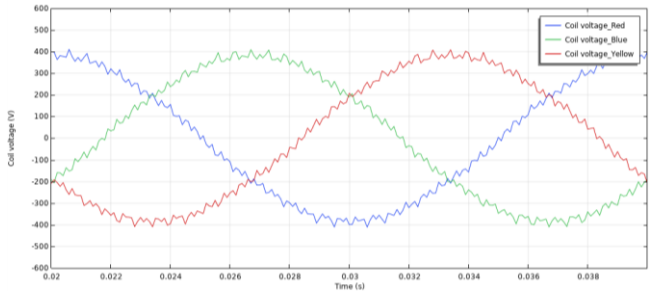


(a) 2-pole stator terminal voltage with 6-pole loaded

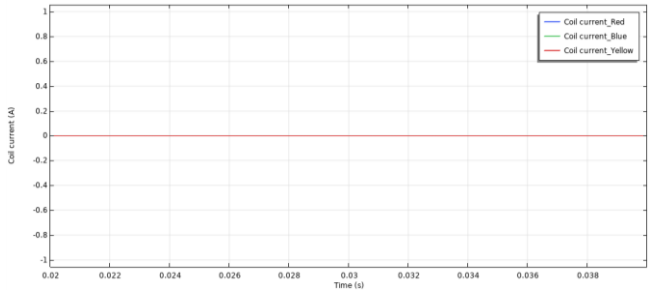


(b) 2-pole stator terminal current with 6-pole loaded

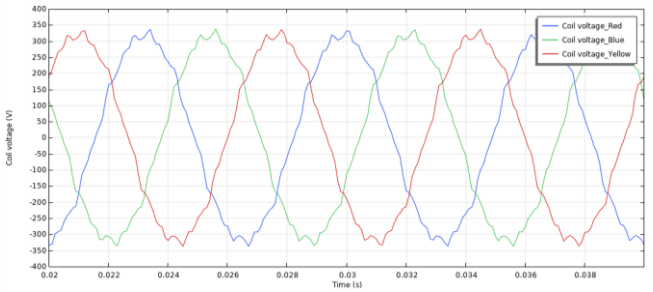


(c) 6-pole stator terminal voltage with 6-pole loaded

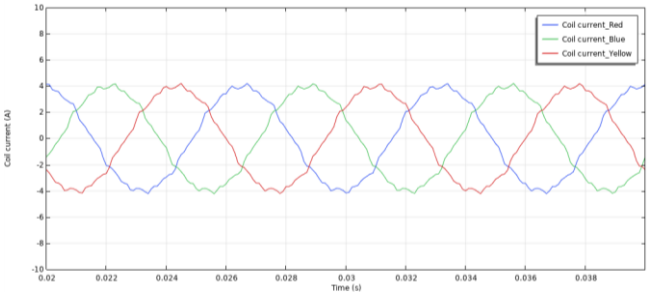


(d) 6-pole stator terminal current with 6-pole loaded

Fig. 12. Terminal voltage & current with 6-pole loaded

For both 2-pole winding with 60 Ω resistive load and 6-pole winding with 80 Ω resistive load, the terminal voltage and current are shown in Fig. 13. Compared to each winding working separately, the stator voltage and current with dual load are still similar to the results with the single load conditions, which illustrates that the 2-pole generator does not affect 6-pole generator and vice versa.

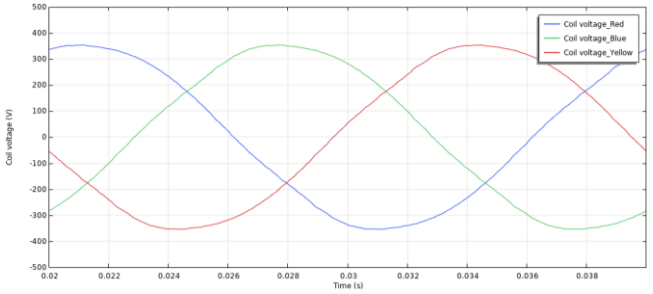


(a) 2-pole stator terminal voltage with 2-pole and 6-pole loaded

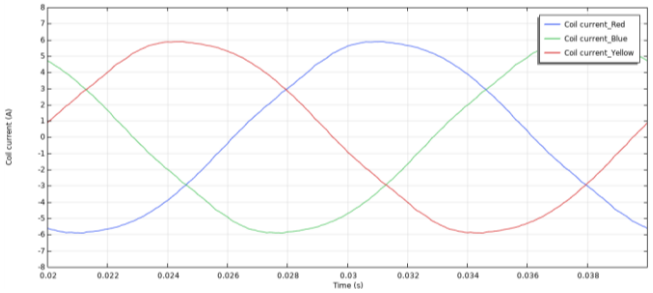


(b) 2-pole stator terminal current with 2-pole and 6-pole loaded

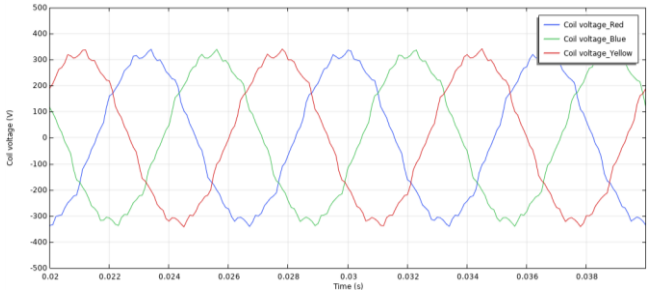


(c) 6-pole stator terminal voltage with 2-pole and 6-pole loaded

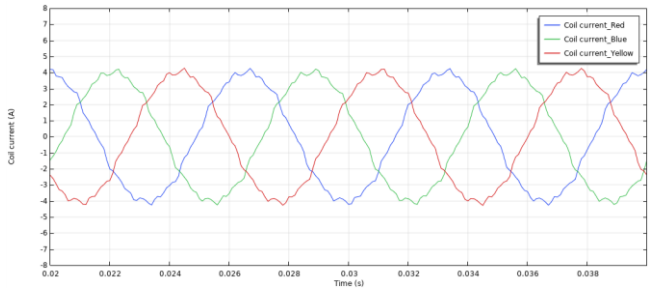


(d) 6-pole stator terminal current with 2-pole and 6-pole loaded

Fig. 13. Terminal voltage & current with 2-pole and 6-pole loaded

The simulation results in this section show the rated operation conditions when either and both windings are loaded. The 2-pole winding has 354 $V_{peak}$, 5.9 $A_{peak}$ and 3 kW rated power. The 6-pole winding has 340 $V_{peak}$, 4.2 $A_{peak}$ and 2 kW rated power. Once the dual wound machine is integrated into an overall electric ship system, the propulsion segment will feed power electronic converters to implement the propeller drive systems. The ship service systems may rectify the power into DC networks. The generator designed in this paper ensures the important condition that the two systems can operate independently. Conclusion

This paper demonstrates a dual wound machine with 2 and 6-pole windings, which can generate two independent power supplies for an IFEP ship system. Analytical calculations and 2D FEA COMSOL simulation are both applied to investigate the generator performance. Based on the harmonic analysis and finite element modelling results, the two outputs are fully electromagnetically decoupled. Further practical experiments will be performed using the model machine and the design described in this paper.

## VI. References


[1] R. T. Meyer, R. A. DeCarlo, S. Pekarek, and C. J. Doktorcik, "Gas turbine engine behavioral modeling," *Journal of Engineering for Gas Turbines and Power*, Dec. 2015.

[2] A. K. Adnanes, "Maritime electrical installations and diesel electric propulsion," ABB report/Lecture note NTNU, 2003.

[3] J. F. Hansen and F. Wendt, "History and state of the art in commercial electric ship propulsion, integrated power systems, and future trends," *Proceedings of the IEEE*, vol. 103, no. 12, pp. 2229-2242, Dec. 2015.

[4] N. Doerry, J. Amy and C. Krolick, "History and the status of electric ship propulsion, integrated power systems, and future trends in the U.S. navy," *Proceedings of the IEEE*, vol. 103, no. 12, pp. 2243-2251, Dec. 2015.

[5] H. Pestana, "Future trends of electrical propulsion and implications to ship design," *Maritime Technology and Engineering*, pp. 797-803, 2014.

[6] J. M. Apsley, A. Gonzalez-Vill asenor, M. Barnes, A. C. Smith, S. Williamson, J. D. Schuddebeurs, P. J. Norman, C. D. Booth, G. M. Burt and J. R. McDonald, "Propulsion drive models for full electric marine propulsion systems," *IEEE Transactions on Industry Applications*, vol. 45, no. 2, pp. 676-684, Mar. 2009.

[7] G. Sulligoi, A. Vicenzutti and R. Menis, "All-electric ship design: from electrical propulsion to integrated electrical and electronic power systems," *IEEE Transactions on Transportation Electrification*, vol. 2, no. 4, pp. 507-521, Dec. 2016.

[8] W. A. Hill, G. Creelman and L. Mischke, "Control strategy for an icebreaker propulsion system," *IEEE Transactions on Industry Applications*, vol. 28, no. 4, pp. 887-892, Jul. 1992.

[9] I. M. Elders, P. J. Norman, J. D. Schuddebeurs, C. D. Booth, G. M. Burt, J. R. McDonald, J. Apsley, M. Barnes, A. Smith, S. Williamson, S. Loddick and I. Myers, "Modelling and analysis of electro-mechanical interactions between prime-mover and load in a marine IFEP system," 2007 IEEE Electric Ship Technologies Symposium, Arlington, VA, 2007, pp. 77-84.

[10] C. G. Hodge and J. F. Eastham, "Dual wound machines for electric ship power systems," 2015 IEEE Electric Ship Technologies Symposium (ESTS), Alexandria, VA, 2015, pp. 62-67.

[11] L. J. Rashkin, J. C. Neely, S. F. Glover, T. J. McCoy and S. D. Pekarek, "Dynamic considerations of power system coupling through dual-wound generators," 2017 IEEE Electric Ship Technologies Symposium (ESTS), Arlington, VA, 2017, pp. 493-500.

[12] J. C. Neely, L. J. Rashkin, S. F. Glover, D. G. Wilson, N. Doerrty and T. Mccoy, "Dynamic response evaluation of a 20 Mw scale dual wound machine based power system," Advanced Machinery Technology Symposium Conference, Mar. 2018.

[13] J. D. Schuddebeurs, P. J. Norman, C. D. Booth, G. M. Burt and J. R. McDonald, "Emerging research issues regarding integrated-full-electric-propulsion," Proceedings of the 41st International Universities Power Engineering Conference, Newcastle-upon-Tyne, 2006, pp. 669-673.

[14] E. Mese, M. Ayaz, M. Tezcan, K. Yilmaz and E. Ozdemir, "A permanent magnet synchronous machine with motor and generator functionalities in a single stator core," Compumag, Jul. 2013.

[15] E. Mese, M. Tezcan, M. Ayaz, Y. Yasa and K. Yilmaz, "Design considerations for dual winding permanent magnet synchronous machines," 2012 IEEE Energy Conversion Congr. and Expo. (ECCE), pp. 1894-1901, Sep. 2012.

[16] J. F. Eastham, T. Cox and J. Proverbs, "Application of planar modular windings to linear induction motors by harmonic cancellation," *IET Electric Power Applications*, vol. 4, no. 3, pp. 140-148, Mar. 2010.

[17] C. G. Hodge, J. F. Eastham and A. C. Smith, "The harmonics analysis of machine excitation," Int. Naval Engineering Conf. (INEC), Edinburgh, May. 2012.

[18] J. F. Eastham and C. G. Hodge "The harmonics analysis of machine phase windings," Int. Naval Engineering Conf. (INEC), Glasgow, May. 2014.

[19] Y. Demir and M. Aydin, "A novel asymmetric and unconventional stator winding configuration and placement for a dual three-phase surface PM motor," *IEEE Transactions on Magnetics*, vol. 53, No. 11, Nov. 2017.

[20] Y. Li, Z. Zhu, X. Wu, A. S. Thomas and Z. Wu, "Comparative study of modular dual 3-phase permanent magnet machines with overlapping/non-overlapping windings," *IEEE Transactions on Industry Applications*, vol. 55, no. 4, pp. 3566-3576, Jul. 2019.


## VII. Biographies

**Boyuan Yin** received B.Eng. from the North China Electric Power University in Beijing, China and the University of Bath in the UK in 2018. He is currently under second year Ph.D. study in the University of Bath. His research field is hybrid DC circuit breaker and electric machine design.

**Dr Xiaoze Pei** received the B.Eng. and M.Eng. degrees from Beijing Jiaotong University, Beijing, China in 2006 and 2008, respectively. She received the Ph.D. degree from the University of Manchester, Manchester, U.K. in 2012. She became a Research Associate at the University of Manchester. In 2017, she joined the University of Bath as a Lecturer. Her research interests include electrical power applications of superconductivity, hybrid DC circuit breaker and electric machine design.

**Dr Xianwu Zeng** received his MSc and PhD at the University of Manchester between 2009 and 2014. He had a broad industry experience in power converter design. He was a lead power electronics engineer in GE grid solution before and was responsible to design valve unit for HVDC projects. He was also involved in several automotive projects including kW level DC-DC converter and inverter. In 2019, he joined the University of Bath as a Lecturer. His principle research interests include power electronics, motor drives, hybrid electric vehicles, and renewable energy interface systems.

**Prof Fred Eastham DSc Dr.h.c.** is now an Emeritus Professor at Bath University after being Head of Department, Dean and Pro-Vice-Chancellor there. He is a fellow of the Royal Academy of Engineering and the Royal Society of Edinburgh. He is a consultant to a number of manufacturing companies.

**Chris Hodge MSc** is the Chief Electrical Engineer at BMT Defence and Security. He is an Honorary Fellow of the IMarEST, a Fellow and former elected Trustee of the Royal Academy of Engineering and an Honorary Professor of Engineering at the University of Warwick. He served as the Chairman of the IMarEST Board of Trustees from 2009 to 2016 and has served as its President. He was made an Officer of the Order of the British Empire in Her Majesty the Queen's Birthday Honours in 2015 for services to Royal Navy Engineering.

**Oliver Simmonds MEng MSc** is a Principal Engineer at BMT in Bath, UK. A Chartered Engineer, he has a background in both Mechanical and Electrical Engineering and has lead several major projects ranging from the delivery of a hybrid power and propulsion system for a Naval auxiliary vessel through to a wide range of technology studies and concept development work for future Power & Propulsion systems.